UNIVERSIDAD DE SANTIAGO DE COMPOSTELA
Departamento de Física de Partículas

Implementation of a GEANT4 simulation for the R3B setup (FAIR) (R3BSIM): application to ^{27}P Coulomb dissociation

Saúl Beceiro Novo
Santiago de Compostela, July 2008.

UNIVERSIDAD DE SANTIAGO DE COMPOSTELA

Dolores Cortina Gil, Investigadora Ramón y Cajal del Departamento de Física de Partículas de la Universidad de Santiago de Compostela,

INFORMA:

que la memoria titulada **Implementation of a GEANT4 simulation for the R3B setup (FAIR) (R3BSIM): application to ^{27}P Coulomb dissociation**, ha sido realizada por **Saúl Beceiro Novo** bajo su dirección en el **Departamento de Física de Partículas de esta Universidad**, y constituye el **Trabajo de Investigación Tutelado** que presenta para optar al **Diploma de Estudios Avanzados**.

Santiago de Compostela, 17 de julio de 2008.

Fdo. Dolores Cortina Gil

Fdo. Saúl Beceiro Novo

Contents

Chapter 1

Introduction

During the past decade it has been demonstrated that reactions with high-energy secondary beams are an important tool to explore properties of nuclei far off stability, which allows detailed spectroscopic information to be extracted. High energy beams, in the range of a few hundred MeV/nucleon, allow a quantitative description of the reaction mechanisms, while also having experimental merits, such as the possibility of using relatively thick targets (in the order of 1 g/cm^2). Moreover, due to the kinematical forward focusing, full-acceptance measurements are feasible with moderately sized detectors. This makes it possible to gain nuclear- structure information from reaction studies even with very low beam intensities, as low as few 1 ion/s.

The R3B (Reactions with Relativistic Radioactive Beams) experiment [1] that would be installed at the FAIR (Facility for Antiproton and Ion Research) [2] facility, will address experimental reaction studies with exotic nuclei far off stability, with emphasis on nuclear structure and dynamics. Astrophysical aspects and technical applications are also concerned.

The goal of this work is to implement part of a simulation package (R3BSim) allowing us to study the response of the experimental setup of the future R3B experiment together with the complete description of the physical processes involved. In particular, we will focus on the use of this simulation package to study the present ALADIN-LAND setup in GSI (Germany) [3].

1.1 R3B

The aim of the R3B international collaboration is to design and construct a versatile reaction setup with high efficiency, acceptance, and resolution for kinematically complete measurements of reactions induced by high-energy radioactive beams produced in the

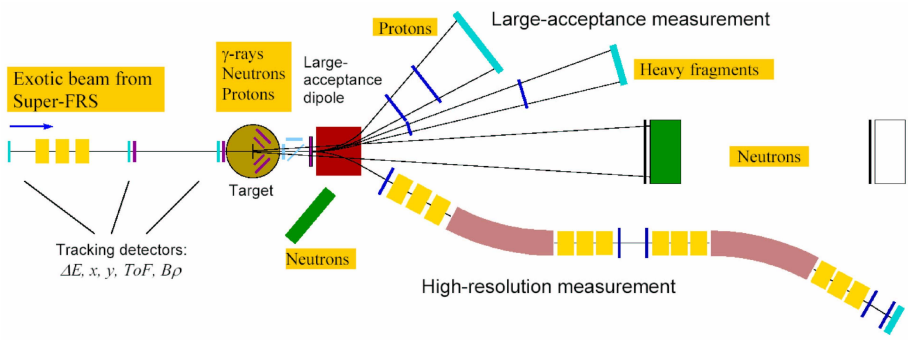

Figure 1.1: Schematic picture of the experimental setup comprising γ-ray and target recoil detection, a large-acceptance dipole magnet, a high resolution magnetic spectrometer, neutron and light-charged particle detectors, and a variety of heavy-ion detectors.

Super-FRS. The experimental configuration is based on a concept similar to the existing ALADIN-LAND [5] reaction setup at GSI introducing substantial improvement with respect to resolution and an extended detection scheme (Fig. 1.1).

The setup is adapted to the highest beam energies (corresponding to 20 Tm magnetic rigidity) provided by the Super-FRS capitalizing on the highest possible transmission of secondary beams. The experimental setup is suitable for a wide variety of scattering experiments, i.e., such as heavy-ion induced electromagnetic excitation, knockout and breakup reactions, or light-ion (in)elastic and quasi-free scattering in inverse kinematics, thus enabling a broad physics program with rare-isotope beams to be performed [1]. The collaboration includes now 52 different institutes from all over the world.

1.1.1 Detection systems

The proposed experimental scheme is based on the existing ALADIN-LAND apparatus which is used successfully in experiments with secondary beams from the FRS facility at GSI. The most essential upgrades concern the silicon target recoil detector, the gamma-ray and light charged particle calorimeter and the two magnetic spectrometers. A schematic view of the R3B experimental setup is shown in Figure 1.1. The incoming secondary beams are tracked and identified on an event-by-event basis. Measurements of the magnetic rigidity Bρ (position measurement at the dispersive focus in the Super-FRS), time-of flight ToF, and energy loss ΔE provide unique isotope identification and momentum determination. Although the secondary beam has a momentum spread of $\pm$2.5%, the momentum will be determined with an accuracy of 10^{-4} (event-wise). After the secondary target, the kinematically forward focused projectile residues are again identified and momentum analyzed. Two modes of operation are foreseen depending on the demands of the experiments:

- A large-acceptance mode: Heavy fragments and light charged particles (i.e. protons) are deflected by a large-acceptance dipole and detected with full solid-angle

acceptance, for most reactions envisaged (left bend in Figure 1.1). Resolutions for velocity and Bρ measurements amount to about 10^{-3} allowing unique identification in mass and nuclear charge for heavy fragments. This part of the setup wii be build in the first term and our simulation is focused on that.

- A high-resolution mode: here, the dipole magnet is operated in reversed mode, deflecting the fragments into a magnetic spectrometer (right bend in Figure 1.1). The envisaged resolution of 10^{-4} will allow, i.e., a precise measurement of the fragment recoil momentum in single-nucleon knockout and quasi-free scattering experiments even for heavy nuclei.

The large gap of the dipole provides a free cone of $\pm$80 mrad for the neutrons, which are detected in forward direction by the large area neutron detector (new LAND). At beam energies around 500 MeV/nucleon, this corresponds to a 100% acceptance for neutrons with kinetic energies up to 5 MeV in the projectile rest frame. Depending on the requirements on resolution and acceptance, the detector with an active area of 2x2 m^2 is placed at a distance of 10 m to 35 m from the target.

The target is surrounded by a γ-ray and light charged particle calorimeter. Some of the planned experiments envisage a high-total-absorption efficiency calorimeter whereas others would demand its use as a high energy resolution spectrometer.

For elastic, inelastic and quasi-free scattering experiments or charge-exchange reactions, liquid hydrogen or frozen hydrogen targets are considered. Recoiling protons and neutrons are detected by a Si-strip array and plastic scintillators, respectively. High energy protons would be stoped by the calorimeter. For measurements at low momentum transfer, the use of an active target is foreseen.

Fast neutrons stemming from (p,pn) type knockout processes can be measured by placing part of the LAND detector at angles around 45 degrees. The Si-strip array is also used as a high-granularity multiplicity detector array for measuring charged particles from the fire-ball, created in semi-peripheral collisions.

1.1.2 Present work

After this brief introduction we will describe in the second chapter the simulation package R3BSim (originaly developed by H. Alvarez [4]) and its application to the current setup ALADIN-LAND (GSI).

The third chapter will be devoted to the application of the simulation package, first to perform some efficiency studies previous to the realisation of a given experiment, and then the implementation of a momentum reconstruction method needed for the analysis

of the measured data after the experiment. Conclusions will be briefly outlined in the last chapter.

Chapter 2

R3BSim

2.1 Introduction

R3BSim is a simulation code particularly developed for the future R3B setup at FAIR. R3BSim is a pure GEANT4 (G4)-ROOT program that features a multihit data structure ready for event analysis and a modular geometry description that allows the integration of new detectors.

2.2 Simulation package

In the R3BSim code most of the R3B detectors are implemented and also the present ALADIN-LAND setup at Cave C (GSI) (detailed description in next section). The program is written in C++; ROOT libraries are included allowing a fully integrated analysis interface: all the detectors are in a single TTree with individual branches for every detector, each one made of collections of detector hits (TClonesArray).

The simulation includes a large set of materials for the detectors and the environment that can be easily exchanged when needed. It has a messenger for users that allows to do important changes in the configuration during the execution of the program (no need to recompile).

Regarding the physical processes, G4 allows and enforces a full customization of the physics description, providing different physics lists that can be chosen by the user, for electromagnetic processes, hadronic, etc (see appendix for an example of a physics list).

Once we have a realistic description of the experimental setup and the physics, we need to simulate the incoming particles or beam. For that purpose, different event generators

are available, like for instance single particles (protons, neutrons, gammas...) at different conditions (initial point, direction, energy...). Other more complicated generators are being developed, in particular in this work we have used one based on theoretical calculations for the Coulomb dissociation of ^{27}P (explained in section 2.4). The different steps performed during the simulation process include:

- The starting point of the simulation (from where the particles are launched) defines the primary vertex. From that point, every particle is tracked during its flight.
- The simulation calculates the new energy and direction after each step. The step length is defined internally by the program taking into account the energy of the particle and the material that is crossing.
- The particles pass through the detectors leaving a signal that is recorded there. This information is processed in an event by event basis.
- All the recorded information is collected for thousand of events altogether. Afterwards we manage to access this information and reconstruct all the hits doing iterations with analysis algorythms. This last step is done externally.

2.3 Validation of energy loss measurements in GEANT4

To validate the internal G4 (version 4.9.1p01 in this case) energy loss calculation we have performed a simple simulation covering different ions ranging from H to U at different energies impinging different materials. This simulation includes a simple 1 cm^2 square box located inside a vacuum volume. The results are compared to the ones obtained using another code providing very accurate energy loss estimations for relativistic heavy ions: ATIMA.

ATIMA [6] is a program developed at GSI which calculates various physical quantities characterizing the slowing-down of protons and heavy ions in matter for specific kinetic energies ranging from 1 keV/u to 450 GeV/u such as stopping power, energy loss, energy-loss straggling, angular straggling, range, range straggling and beam parameters (magnetic rigidity, time-of-flight, velocity, etc.)

2.3.1 Energy measurements

To obtain the energy loss in the G4 simulation, the initial (before entering the matter box) and final energy (after exiting the box) are measured. The selected events are the ones coming from a primary reaction and having crossed the whole target avoiding contributions coming from backward ions.

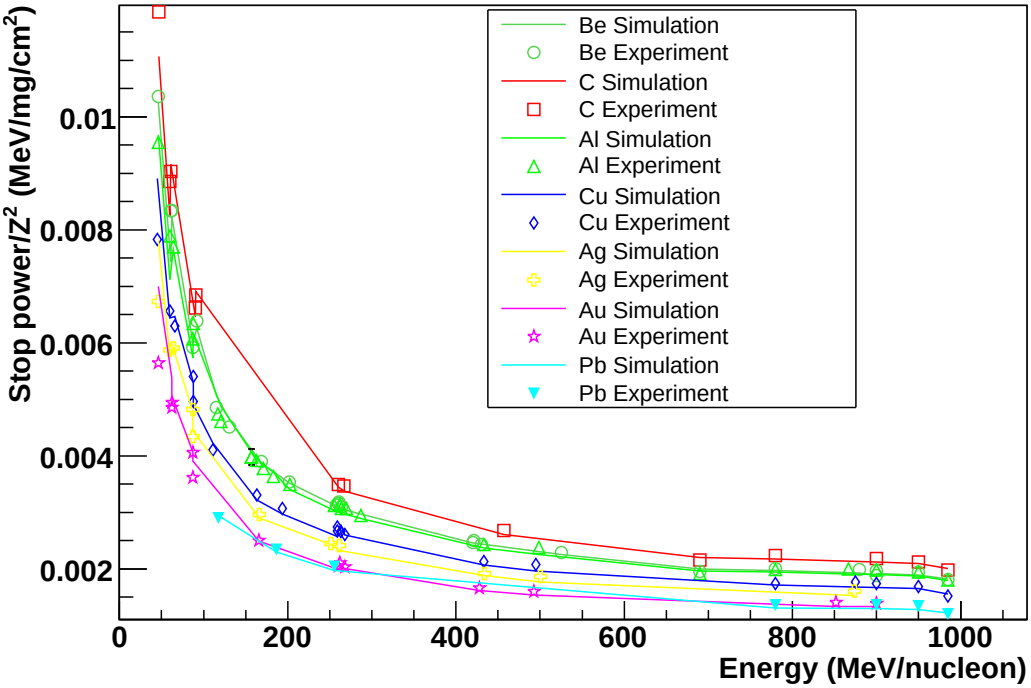

Figure 2.1: *Experimental and calculated (G4) stopping power for different projectiles impinging in several targets as a function of the projectile incident energy per nucleon*

The energy loss measurements are made in series of 1000 ions and normalised to the density and thickness of the target providing stopping powers.

While running the simulation for heavy ions, some problems were found. A function called G4BinaryLightIonreaction() is used by the constructor of the Binary Cascade proccess (EmBinaryCascadeBuilder.cc), but that function can only be used for some projectiles with a given mass. That function is then replaced by the G4WilsonAbrasionModel() that can be used for all kind of ions and targets.

2.3.2 Comparison between GEANT4, ATIMA and experimental data

All the simulated processes have been compared to experimental values in a quite broad energetic regime and different ions ranging from B to Pb. In figure 2.1 we plot the energy dependence of the stopping power for all the targets (normalising to Z^2 of the projectiles) comparing the experimental values (crosses) [8, 9] with the simulated ones (lines) .

Another view of the same results is shown in figure 2.2 that indicates the percetual difference between G4 stopping power evaluation and experimental data for all the stud-

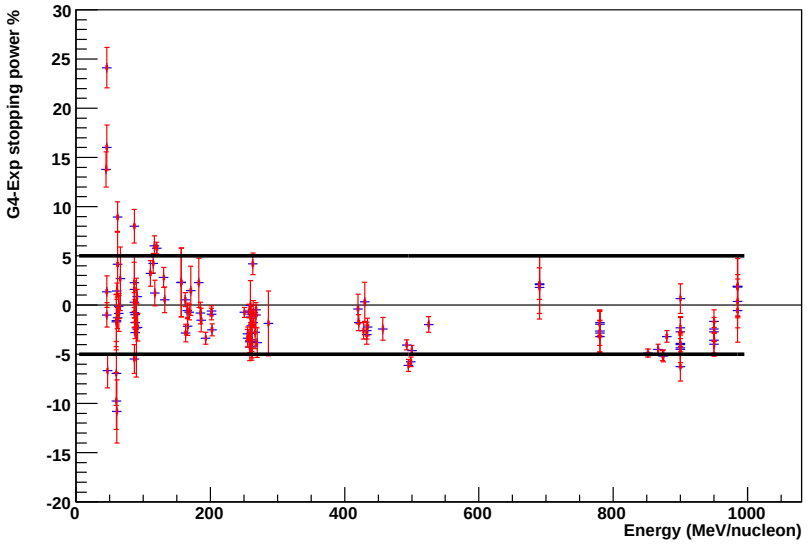

Figure 2.2: *Percentual difference between experimental and calculated by G4 stopping power as a function of the incident ion energy per nucleon.*

ied targets. We can observe that most of the experimental and simulated values are in close agreement but 7 points. All of them correspond to measurements of Ni and Xe at low energies (around 60 MeV) measured in the same experiment [9], indicating a possible systematic error in those measurements.

In order to further clarify this discrepancy, we decided to compare the G4 simulation with same ATIMA calculations (see figure 2.3). The 7 points that were identified as not following the G4 predictions are neither reproduced by ATIMA. This fact confirms our suspect of experimental systematic errors associated to these measurements.

The average G4 precission for energies of few hundreds of AMeV is better than 5%. The G4 simulation in the ranges from 50 to 900 MeV and for projectiles from Z=1 to 90 and targets from Z=4 to 82, is more precise than the GEANT3 one but it is still worse than the ATIMA values. The comparison shows that for G4 the precision obtained is around $3-4\%$ for energies around 500 MeV/nucleon, accurate enough for the purpose of this study. For other purposes, when higher precision is needed other codes like AMADEUS or ATIMA are needed; see [7] and references therein.

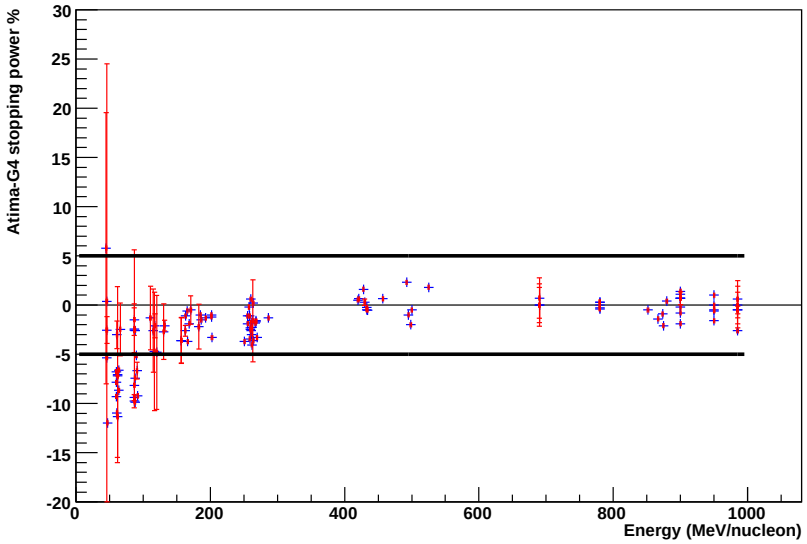

Figure 2.3: *Percentual difference between calculated by ATIMA and calculated by G4 stopping power as a function of the incident ion energy per nucleon.*

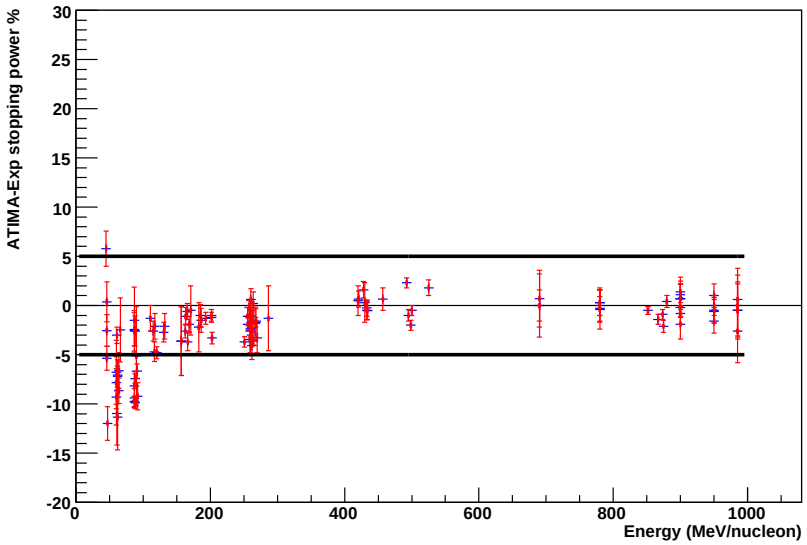

Figure 2.4: *Percentual difference between experimental and calculated by ATIMA stopping power as a function of the incident ion energy per nucleon.*

2.4 Application to the current setup at cave C (GSI)

As said before, R3BSim package can also be used for the current ALADIN-LAND setup placed in Cave C at GSI. In figure 2.5 we show the whole ALADIN-LAND setup as it was

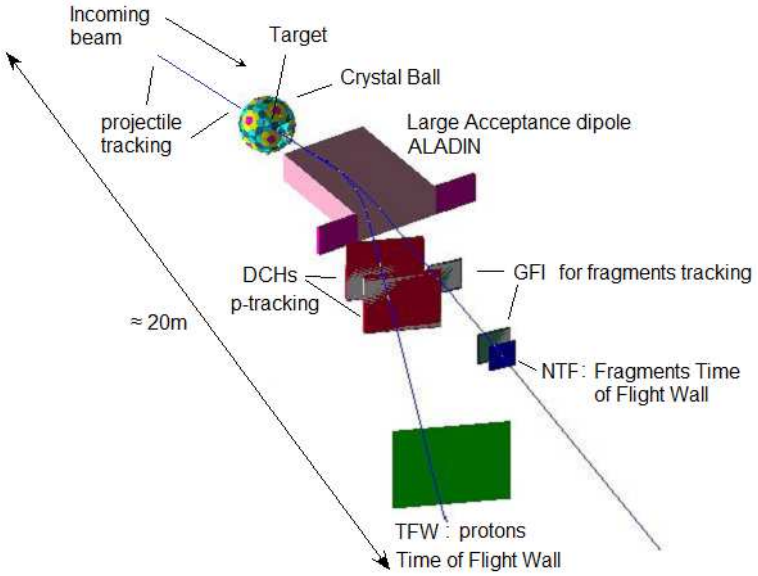

Figure 2.5: ALADIN-LAND experimental setup configuration for ^{27}P C.D.

used for Coulomb dissociation (CD) of ^{27}P in a ^{26}Si and a proton (experiment S223, GSI, May 2007). In next section we briefly describe the different detectors that are included in the simulation and used to extract conclusions about the geometrical efficiency and momentum reconstruction resolution for the different reaction fragments.

2.4.1 Implementation of the setup in the simulation

Following figure 2.5 the experimental setup includes:

1. An incoming vacuum pipe which goes up to the entrance of the magnet, with a 250 μm iron exit window. This pipe follows the beam direction, this is z axis.
2. Within the vacuum pipe, there is a Pb target, where the C.D. reaction takes place. The thickness of the target can be easily exchanged while running the simulation.
3. Behind the target we have a silicon multistrip detector (SSD) in order to measure the (x, y) position of the produced fragments. The characteristics of the detector are summarized in table 2.1.

Active area $x \times y$ (cm)	$7. \times 4.$
Media	Si
Thickness (cm), (mg/cm^2)	0.03, 69.9
Spatial resolution, σ (cm)	0.003

Table 2.1: *Characteristics of the silicon multistrip detector used in the ^{27}P C.D. experiment*

4. After that we simulate the gap of the ALADIN dipole (155. × 50. × 230. cm) filled with He in order to reduce the angular straggling and rotated 7.2 degrees with respect to beamline. The iron constrains of the magnet have been also included in the simulation.

5. We have also considered two different branches for the two CD fragments, composed by tracking detectors and a TOF wall. They follow respectively the trajectories of the ^{26}Si ions and protons. The first one is rotated 16 deg respect to the z axis of the beamline and the second one, 32 deg.

6. The tracking detectors placed after the magnet are two fiber detectors (GFI) for the ^{26}Si ions and two drift chambers (DCH) for the protons. Their characteristics are given in tables 2.2 and 2.3.

Active area $x \times y$ (cm)	50. × 50.
Media	*Scintillator plastic* C_9H_{10}
Thickness (cm), (mg/cm^2)	0.1, 103.2
Spatial resolution, σ (cm)	0.1

Table 2.2: *Characteristics of the GFI detectors used in the* ^{27}P *C.D. experiment.*

Active area $x \times y$ (cm)	102.8 × 80.4
Media	50% Ar + 50% C_2H_6
Thickness (cm), (mg/cm^2)	8., 8.
Spatial resolution, σ (cm)	0.02

Table 2.3: *Characteristics of the drift chambers used in the* ^{27}P *C.D. experiment.*

We have also included Al frames for these detectors and two 12 μm mylar layers for each DHC, limiting the active volume. The drift chambers for protons are placed as close as posible to the magnet in order to optimise the geometric efficiency.

7. Finally, two TOF detectors have been included. The TOF wall for the protons will be used in the experiment only as trigger whereas the one for the ^{26}Si will provide an aditional identification of the ions by measuring their velocities. In principle, the identification of the ^{26}Si ions will be done by means of the energy loss in the silicon detector, but as this measurement is not expected to be accurate enough, they will be also identified using the TOF technique.

All the detectors are placed in a "world" volume filled with air. Every position, size, and material can be easily exchange within the simulation without even recompiling using a Messenger routine that is implemented, so the setup can be easily adapted for any experiment.

The response of the detectors is simulated in a simple way: when a hit takes place in one detector the position, energy or time signal is recorded. Then we apply a gaussian random around the mean value taking into account the precision of the detector. The signals are then recorded into a root tree that can be analysed in the same way as a real experiment.

2.4.2 Magnetic field of the ALADIN dipole

The magnetic field in the simulation can be easily chosen between different possibilities. At the moment 3 choices are implemented:

1. ALADIN measured magnetic field.
2. R3B magnetic field.
3. Constant magnetic field in the y direction.

In this work we are using ALADIN magnetic field, which comes from experimental maps measured at GSI. We used a field map where the x, y and z dimensions of the magnet were covered by intervals of 5 cm. Our code gets the magnetic field value for a given point $\vec{r_0} = (x_0,\ y_0,\ z_0)$ within the magnet by an interpolation in the mentioned map, using the equation 2.1.

$$\begin{aligned} B_i(\vec{r_0}) &= (1-t)(1-u)(1-v)B_i(\vec{r_1}) \\ &+ (1-u)(1-v)B_i(\vec{r_2}) \\ &+ tu(1-v)B_i(\vec{r_3}) \\ &+ tuvB_i(\vec{r_4}) \\ &+ (1-t)u(1-v)B_i(\vec{r_5}) \\ &+ (1-t)uvB_i(\vec{r_6}) \\ &+ (1-t)(1-u)vB_i(\vec{r_7}) \\ &+ t(1-u)vB_i(\vec{r_8}) \quad i = x,\ y\ z \end{aligned} \tag{2.1}$$

where

$$\begin{aligned} t &= \frac{x_0 - x_{lt}}{x_{gt} - x_{lt}} \\ u &= \frac{y_0 - y_{lt}}{y_{gt} - y_{lt}} \\ v &= \frac{z_0 - z_{lt}}{z_{gt} - z_{lt}} \end{aligned} \tag{2.2}$$

and

$$\begin{aligned}
\vec{r_1} &= (x_{lt},\ y_{lt},\ z_{lt}) \\
\vec{r_2} &= (x_{gt},\ y_{lt},\ z_{lt}) \\
\vec{r_3} &= (x_{gt},\ y_{gt},\ z_{lt}) \\
\vec{r_4} &= (x_{gt},\ y_{gt},\ z_{gt}) \\
\vec{r_5} &= (x_{lt},\ y_{gt},\ z_{lt}) \\
\vec{r_6} &= (x_{lt},\ y_{gt},\ z_{gt}) \\
\vec{r_7} &= (x_{lt},\ y_{lt},\ z_{gt}) \\
\vec{r_8} &= (x_{gt},\ y_{lt},\ z_{gt})
\end{aligned}$$

The subscripts gt and lt make reference to the values of x, y and z in the field map which are next to x_0, y_0 and z_0, being $x_{lt} < x_0 < x_{gt}$, $y_{lt} < y_0 < y_{gt}$ and $z_{lt} < z_0 < z_{gt}$.

For ALADIN the most important one is the vertical B_y component of the field, which is constant along the x, y and z directions and responsible of the dipolar behaviour of the magnet. The B_x component of the field is neglegible and B_z is antisymmetric in the y and z coordinates. Taking this into account, the most relevant effect of the magnetic field over the ion trajectories will be a deflection in the x direction, depending on the ion and its energy as it is shown in equation 2.3, where m is the rest mass of the ion, q is its charge and ρ is the radio of curvature in the magnetic field B. We will use this effect to reconstruct the proton momentum.

$$\rho = \frac{\gamma m v}{B q} \tag{2.3}$$

It is clear that a bigger deflection will result in a better separation of the proton trajectories with different momentum and will improve the resolution in the momentum reconstruction. We have selected for the simulations the maximum intensity of the field that allowed the transmission of the protons, without hitting the magnet side walls. We see in equation 2.3 that the magnitude of the field has to be modified each time we consider a different energy in order to preserve the deflection power.

2.4.3 Example of Coulomb dissociation

We want to study the C.D. reaction of the exotic ion ^{27}P. For that purpose, we use the simulated setup described before for Cave C at GSI. The reaction $^{26}Si(p\gamma)^{27}P$ is relevant to the synthesis of ^{26}Al that is a rare isotope of astrophysical interest. Experimental

observations have found that the amount of this isotope produced in stellar scenarios is surprisingly high according to the theoretical expectations. The C.D. [10],[11],[12],[13] studies the inverse reaction ($Pb(^{27}P, p^{26}Si)Pb$): P ions bombard the lead target (high Z), and the Coulomb field of the electrons of the target excites the P which afterwards decays into a proton and a Si ion. The Coulomb field plays a role of a virtual photon in the reaction. Previous measurements of this reaction [14] estimate a cross section that amounts around 15 mb. The same experiment has been also performed recently at GSI where we expect to get higher statistics and better resolution. The simulation of this experiment is the main topic of this work.

The starting point of a G4 simulation is the implementation of an event generator that in this case is a file containing energy-momentum values for the fragments produced in the C.D. of ^{27}P following the theoretical estimations by Stefan Typel.
The event generator is based on a data file where the 4-momentum of the proton and of the ^{26}Si are stored for 10^5 CD events for ^{27}P at 500 MeV/nucleon, which can be randomly triggered.

As we try to perform a realistic simulation, the emission point within the target was forced to follow a gaussian distribution with $FWHM = 1\ cm$ in the x and y coordinates, reproducing the expected beam profile. For the z coordinate, the location straggling was taken into account by means of a step function covering the thickness of the Pb target.
In this case, we have simulated the ^{26}Si and the proton coming out from the ^{27}P CD through the ALADIN setup.

Chapter 3

Application of the simulation package to the real experiment

3.1 Introduction

While preparing an experiment the use of adequate simulation tools is a key issue. The exact location of detectors needs to be optimised in order to obtain the maximum geometrical efficiency for the measurements of interest. In this work, we present an application of detector position determination that maximises the geometrical efficiency for the case of fragments coming from the C.D. of ^{27}P.

Another important feature of a general purpose simulation package is the development of algorithms that can be further used in the analysis. We have also developed in this work a momentum reconstruction method that allows to calculate the momentum of the measured particles, one of the key observables in the final data analysis.

3.2 Geometrical efficiency

As it has been said before, is very important to optimise the experimental setup for the particular reaction that wants to be measured. In our case we were interested in the study of C.D. of ^{27}P. Prior to the experiment the only possibility of testing the optimum detector location is the use of simulated data. We have produced ^{27}P C.D. fragments (protons and ^{26}Si ions), using the theoretical model by S. Typel. Introducing these simulated data in the G4 package we can calculate how many of the launched protons hit the DCH detectors and TOF wall in coincidence with an ion hit in the GFI detectors and NTF. This selection corresponds to a filter that guarantees that we have a proper fragment coming from C.D.

This procedure gives us the geometrical efficiency of the setup for this particular reaction.

In our case the optimum configuration corresponds to a geometrical efficiency of roughly 98% when we placed the detectors in the positions given in table 3.1 (all of them referred to the center of the target and rotation angle respect to Y axis):

Detector	x (cm)	y (cm)	z (cm)	$\theta(deg)$
DCH1	128.7	0	443.9	31
DCH2	169.1	0	535.8	31
TOF	419.7	0	952.4	31
GFI1	73.7	0	525.5	16.7
GFI2	141.8	0	727.3	16.7
NTF	151	0	758	16.7

Table 3.1: *Optimised positions of the detectors that result in a setup geometrical efficiency of 98% for ^{27}P C.D. fragments*

We have also discovered with this simulation that the first DCH should be shifted from the proton branch[1] line around 13 cm in order to avoid interferences with the first GFI active area.

3.3 Development of analysis algorithm

In the analysis of the C.D. experiment, one of the most important observables is the momentum of the fragments, in particular the momentum of the protons. In this work we have developed a method that allows to perform a momentum reconstruction by using the simulation package. This simulation also allows us to test the sensitivity of the reconstruction method to different parameters. It also provides the final resolution that one expects to achieve in the momentum reconstruction.

3.3.1 Backward momentum reconstruction method

Previous simulation work performed in the framework of GEANT3 [7] taught us that the final momentum resolution varies for different reconstruction methods. The best results achieved in this work corresponded to the option of using a backward tracking technique to reconstruct the momentum of fragments.

[1]The proton branch is the line that the protons follow after being bent in the magnet. For ^{27}P C.D. at 500 MeV with a current of about 1800A in ALADIN, this branch would be bent 31^0 respect to the main beam direction whereas the ions would be bent just 16.7^0

For the backward tracking we exploit the proton branch information, in particular the measurement of the position in both DCH.

The reconstruction comprehends the following points:

- The first step would consist on the calculation of the direction in which the protons should be launched using the measured positions recorded in both DCH (x_1,y_1), (x_2,y_2):

$$\theta = atan\frac{\sqrt{(x_2 - x_1)^2 + (y_2 - y_1)^2}}{z_2 - z_1} \tag{3.1}$$

$$\phi = atan\frac{y_2 - y_1}{x_2 - x_1} \tag{3.2}$$

$$\begin{aligned} Px &= Psin\theta cos\phi \\ Py &= Psin\theta sin\phi \\ Pz &= Pcos\theta \end{aligned} \tag{3.3}$$

- Then we proceed to run the simulation backwards, meaning that now the starting point for the protons would be the measured position in the last DCH.

- We invert the magnetic field. With this condition we launch the protons and check if they reach the starting point in the target.

- A necessary condition is to ensure that the proton energy loss before entering the magnet in the backward case is equivalent to the energy loss suffered in the forward case. To achieve this effect when we run backwards, we place a lead box with a thickness that is half of the real target before entering the magnet.

- Next step is to fix the proper proton momentum. To get this value we iterate within a momentum range according to the theoretical expected values. The right momentum corresponds to the one giving a right position measured in the target within a confident range of $100\mu m$. At the moment, the position in target is being measured by 2 scintillators in front of the target that do not have very good precision. We are working now to include in the methode the positions measured using a silicon strip detector (2.1) that was located just after the target with much better precision. This detector has been used for the first time in the C.D. experiment we are presently working in the readout and calibration of data.

- The last step is to compare the measured momentum values with the real ones in order to evaluate the resolution we get with that method ($\Delta p/p = (P_{real} - p_{sim}/p_{real})$).

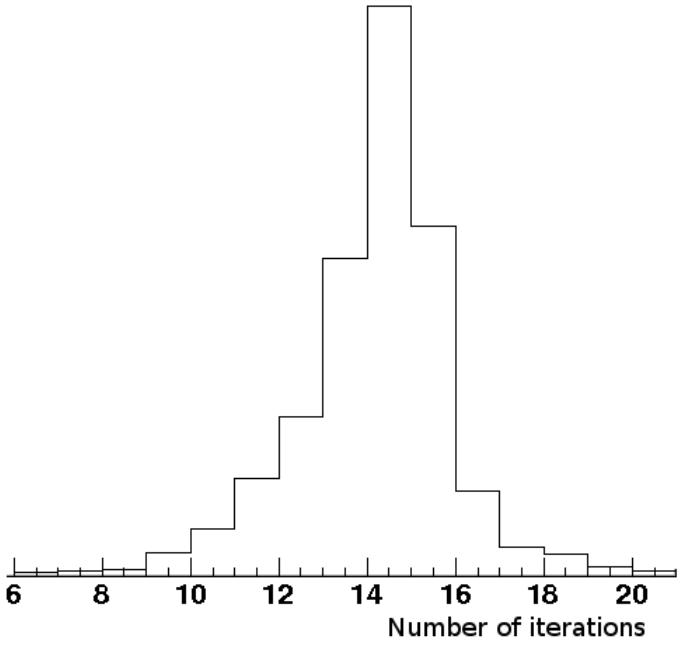

Figure 3.1: Number of iterations needed in the backtracking reconstruction methode in order to have convergency for the momentum calculation for the particular case of simulted protons coming from C.D of ^{27}P

3.3.2 Testing the method with simulated data

A first test for the reconstruction method is to calculate the momentum resolution achieved for the case of simulated protons. For this, we run the R3BSim program for C.D. at cave C in forward mode and we record positions corresponding to emitted protons both in target and in DCH. Then, we use the positions and we apply the backward momentum reconstruction routine presented in previous section. We finally compare the calculated value for the reconstructed momentum with the nominal value given by the simulation. The method converges in about 14 iterations (see fig 3.1) obtaining a momentum resolution of roughly a 0.5% (see fig 3.2) that is accurate enough for our analysis purposes and it is comparable to previous results achieved using Geant3 [7].

In figure 3.3 we compare the reconstructed momentum distribution with the original one corresponding to the theoretical spectrum (from S. Typel code) that is used as input for the simulation. The agreement between both distributions is quite good.

The accuracy of the method depends basically on 2 factors: the precision of the position and magnetic field measured values.

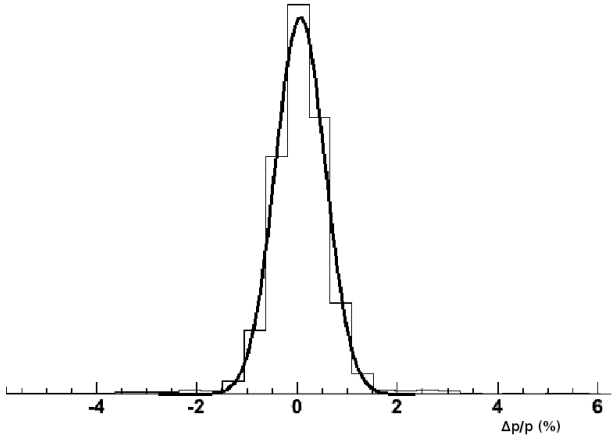

Figure 3.2: Resolving power for the momentum obtained by using the backtracking momentum reconstruction method with simulated protons coming from C.D. of ^{27}P. The result yields a Δp/p value with FWHM of 0.5% that would be in principle precise enough for our purpose

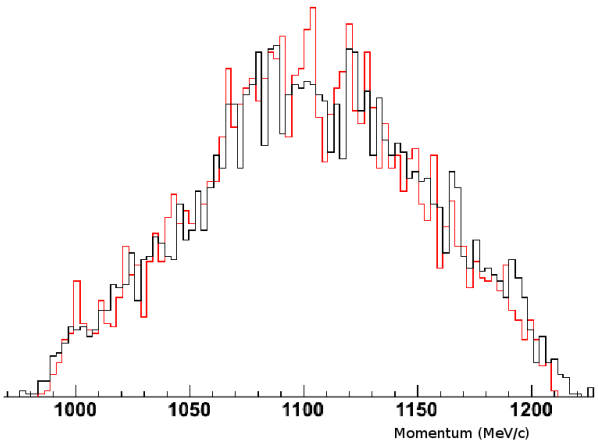

Figure 3.3: Momentum distribution for protons coming from C.D of ^{27}P. In red we plot the distrubution obtained with the reconstruction method. In black the distribution calculated according to S. Typel model.

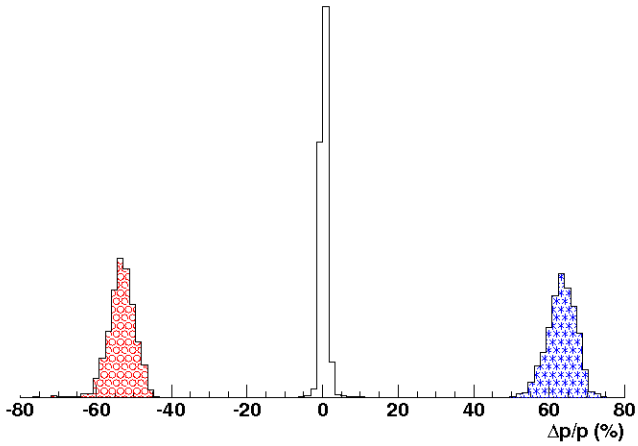

Figure 3.4: Resolving power for the momentum obtained by using the backtracking momentum reconstruction method with simulated protons at 500 MeV. The white histogram corresponds to the case of using positions provided by the simulation and has a FWHM of 0.5%. The histogram filled with red circles corresponds to the same calculations but with positions shifted by -10% in x and yields an offset in momentum of -53% respect to the nominal value and a FWHM of 3.5% The histogram filled with blue stars corresponds to the equivalent shift +10% in x and yields an offset in momentum of +63% and a FWHM of 3.1 %

We can do a rough test on how much those variables affect the reconstruction method in the regions we are working.

- For the postition sensitivity we performed the backward momentum reconstruction using the position coming from the simulation and then varying this value by ±10% in x. We observed an offset of around -53% when shifting x to the left and +63% for an equivalent shift to the right in x (see fig 3.4). This result tells us that the method is highly sensitive to the position measurement.

  As a conclusion a small error in the experimental position would yield an important error in the final momentum reconstruction as well as a wrong momentum resolution asignement.

- For the magnetic field sensitivity we run the simulation with the nominal magnetic field value first (for protons at 500 MeV it corresponds to a current of 1800 A for ALADIN magnetic field) and then we repeat the measurement by using a magnetic field different by ± 10%. We observed a non-linear behaviour: for the magnetic field reduction we get an offset in the momentum calculation of around 3% whereas for the highest B value the offset is 14% in momentum. This indicates the importance of a precise knowledge of the experimental B value applied and its precision.

3.3.3 Testing the method with real data

The next step is to test the method using real data. The first attemp is to use data from a test run where we had a pure proton primary beam at a known nominal energy. This run was taken at GSI (ALADIN-LAND setup) in may 2007 with protons in an energy range from 200 to 540 MeV. In this work, we only use the runs at 460 MeV, 480 MeV, 500 MeV and 540 MeV.

The first step consists on the analysis of this data. To get the position of the hits in the DCH we need to use a software called land02 that is being develloped by the ALADIN-LAND collaboration and that allows to unpack the experimental data and also to calibrate the detectors.

Once we have the (x,y) position for the proton hits in DCH we are in a similar situation as the one described in previous section for simulated protons. Next step will consist on calculating the direction of each proton track in order to make the backward iteration for the momentum calculation.

The accuracy of the method depends dramatically on the precision of the position measurement in the different hitted detectors. We must be careful with using the same reference points for both simulated and real detectors, otherwise the result of the analysis will be seriously compromised.

We do not have at the moment precise enough measurements of the real location of the detectors and so far we can only test the convergency of the method. However we cannot give absolut momentum values with more precision than 10% as of course the method is very sensitive to small position variations.

In figure 3.5 we can see the reconstructed momentum for protons of 460 MeV, 480 MeV, 500 MeV and 540 MeV. In all cases the obtained resolving power $\Delta p/p$ is 0.48%, the same order of magnitude as we should expect comparing to the simulated data. Neverthless we get a 10% offset with respect to the expected momentum value. According to what we presented in previous section, this 10% error in the momentum assignement may come from a 1% error in the precision of the positioning of the detectors.

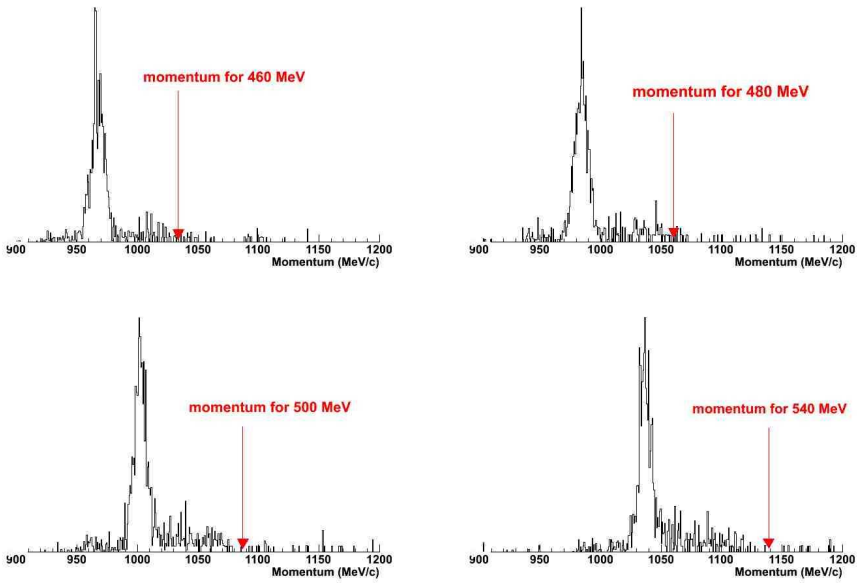

Figure 3.5: Reconstructed momentum using the backtracking reconstruction method for protons of 460, 480, 500 and 540 MeV. An offset of roughly 10% in the mean value is observed with respect to the expected value (marked with an arrow)

Chapter 4

Summary and Conclusions

In this work we have described a general purpose simulation package based in GEANT4 (G4) called R3BSim that can be used for the future R3B setup at FAIR and also for the current ALADIN-LAND setup at GSI.

The simulation provides the whole description of the different detectors (materials, location and response) as well as the physical processes that take place during the experiment. All the processed events are recorded in root files that can be analysed externally.

We have applied the simulation to the study of the coulomb dissociation (C.D.) of ^{27}P. An external event generator based on a theoretical model and developed by S. Typel is used for that purpose.

The accuracy of the simulation for energy loss calculations (G4) has been tested and compare with real data getting precisions ranging from 1 to 5% in the energy range of interest (300-600 MeV/u). This accuracy is shown to be better than estimations of previous versions of GEANT (G3) and thus is precise enough for our studies.

In this work we focused on the application of the simulation to the particular experimental ALADIN-LAND arrangement at GSI for the study of the C.D. of ^{27}P. A detailed description of the experimental setup has been introduced in the R3B simulation framework including the description of the incoming vacuum pipe, target, ALADIN and tracking detectors. With this geometry we have performed a simulation in order to optimise the location of the detectors providing the largest geometrical efficiency (98% in this case for C.D. fragments of ^{27}P at 500 MeV/u).

To reconstruct the momentum of the fragments (protons in this work), a backward tracking algorithm has been implemented. This algorithm takes the measured positions

for protons in both DCH and also the vertex in the target. With the DCH positions we get the direction of the protons after the magnet. Protons are then launched backwards following exactly that direction crossing the magnet again (we invert the magnetic field). We iterate over different values for the momentum until the protons hit in the vertex that had been measured before in the target. This is the reconstructed momentum value.

We have tested the method with simulated protons coming from the C.D. of ^{27}P getting a precision in the momentum mean value of 0.01% and a resolving power $\Delta p/p$ of 0.5% (FWHM). The method was also tested with real protons measured in a parasitic beam at GSI (460, 480, 500 and 540 MeV) getting a similar resolving power $\Delta p/p$ of 0.5%, however, we get an accuracy of only a 10% for the momentum mean value mainly due to incertainties in position measurements.

We have also studied the sensitivity of the method to variations in magnetic field and position measurements. The results show that variations of 10% in magnetic field measurements lead to variations of 10% for the momentum, but for positions the variation is more severe: a 10% variation in position measurement may lead to 50% errors in momentum reconstruction.

We conclude that this is a powerful method that can be easily use in the analysis of an experiment with momentum resolutions of about 0.5%, but taking into account that the precise measurement of the magnetic field and positioning of the detectors is crucial for getting realistic and trustable results.

Appendix A

A.1 GEANT4 Physics Libraries used for the simulations

- G4EmQEDBuilder
- G4EmMuonBuilder
- G4EmHadronBuilder
- G4LowEnergyQEDBuilder
- G4penelopeQEDBuilder
- HadrontherapyIonLowE
- HadrontherapyIonLowEZiegler1977
- HadrontherapyIonLowEZiegler1985
- HadrontherapyIonLowEZiegler2000
- HadrontherapyIonStandard
- ActarSimDecayBuilder
  - G4Decay
- EmhadronElasticBuilder
  - G4HadronElasticProcess
  - G4LElastic
- EmBinaryCascadeBuilder
  - G4BinaryCascade
  - G4ProtonInelasticProcess
  - G4NeutronInelastic
  - G4HadronFission

  - G4LFission
  - G4hadronCaptureProcess
  - G4LCapture

- EmIonBinaryCascadeBuilder
  - G4LDeuteronInelastic
  - G4BinaryLightIonreaction
  - G4TipathiCrossSection
  - G4IonShenCrossSection
  - G4DeuteronInelasticProcess
  - G4LEDeuteronInelastic
  - G4TritonInelasticProcess
  - G4LETritonInelasticProcess
  - G4AlphaInelasticProcess
  - G4LEAlphaInelasticProcess
  - G4HadronInelasticProcess
  - G4BinaryLightIonReaction

- EmHeavyionBinaryCascadeBuilder
  - this item is exactly the same as the previous one only changing G4BinaryLightIonReaction for G4WilsonAbrasionModel that can be used also for heavy projectiles and targets.

- EmGammaNucleusBuilder
  - G4PhotoNuclearProcess
  - G4TheoFSGenerator
  - G4GammanuclearReaction

A.2 Energy Losses Tables

In the tables A.1, A.2, A.3, A.4, A.5, A.6 and A.7 we write all the data used in the analysis: the experimental and the simulated data and also the difference between the simulation codes and the experimental data in percent. The experimental data is taken basically from [8], and [9] (these ones marked with †), and (marked with *). The stopping powers are measured in $MeV/mg/cm^2$

A	proj	$E(MeV/u)$	G4	ATIMA	Exp	%G4	%ATIMA
58	$Ni^{\dagger}$	46	8.038	7.998	8.12	−0.998	−1.501
136	$Xe^{\dagger}$	61	21.676	21.732	24.3	−10.794	−10.565
58	$Ni^{\dagger}$	62	6.454	6.475	6.54	−1.314	−0.992
136	$Xe^{\dagger}$	87	17.527	17.595	17.25	1.606	2.001
58	$Ni^{\dagger}$	92	4.896	4.884	5.01	−2.262	−2.511
197	Au	115.3	31.625	29.584	30.34	4.237	−2.490
208	Pb	130.7	31.201	29.582	30.35	2.806	−2.527
209	Bi	168.8	26.649	26.475	26.84	−0.708	−1.359
208	Pb	201.8	23.648	23.628	23.79	−0.595	−0.677
197	Au	257.7	19.420	19.483	19.54	−0.611	−0.289
58	Ni^{*}	260	2.476	2.464	2.477	−0.032	−0.502
58	$Ni^{\dagger}$	261	2.456	2.459	2.48	−0.939	−0.842
136	$Xe^{\dagger}$	261	9.063	9.171	9.26	−2.118	−0.953
209	Bi	264	21.106	21.179	21.27	−0.768	−0.426
86	Kr^{*}	420	3.193	3.190	3.206	−0.399	−0.491
136	$Xe^{\dagger}$	421	7.169	7.250	7.3	−1.782	−0.682
58	Ni^{*}	430	1.910	1.897	1.904	0.324	−0.335
209	Bi	525.1	15.497	15.878	15.81	−1.977	0.431
18	O^{*}	690	0.127	0.126	0.125	2.164	0.926
136	Xe^{*}	780	5.746	5.806	5.861	−1.949	−0.931
209	Bi	879.6	13.292	13.683	13.73	−3.188	−0.340
86	Kr^{*}	900	2.448	2.437	2.432	0.660	0.234
238	U^{*}	900	16.266	16.840	16.648	−2.293	1.153
197	Au^{*}	950	11.796	12.146	12.124	−2.700	0.188
40	Ar^{*}	985	0.589	0.584	0.587	0.389	−0.359

Table A.1: *Stopping powers for berilium target*

A	proj	$E(MeV/u)$	G4	ATIMA	Exp	%G4	%ATIMA
58	$Ni^{\dagger}$	47	8.679	8.628	9.3	-6.672	-7.219
136	$Xe^{\dagger}$	60	24.036	24.046	25.83	-6.944	-6.904
58	$Ni^{\dagger}$	61	7.179	7.179	7.08	1.408	1.402
136	$Xe^{\dagger}$	90	18.856	18.910	19.3	-2.297	-2.020
58	$Ni^{\dagger}$	91	5.415	5.400	5.37	0.854	0.561
58	$Ni^{\dagger}$	260	2.706	2.709	2.74	-1.226	-1.115
136	$Xe^{\dagger}$	267	9.849	9.965	10.13	-2.765	-1.628
136	$Xe^{\dagger}$	457	7.620	7.695	7.81	-2.428	-1.468
18	O^{*}	690	0.140	0.138	0.138	2.057	0.239
136	Xe^{*}	780	6.339	6.372	6.524	-2.821	-2.317
238	U^{*}	900	17.964	18.497	18.47	-2.735	0.148
197	Au^{*}	950	13.033	13.336	13.256	-1.681	0.604
40	Ar^{*}	985	0.651	0.640	0.64	1.821	0.136

Table A.2: *Stopping powers for carbon target*

A	proj	$E(MeV/u)$	G4	ATIMA	Exp	%G4	%Atima
58	$Ni^{\dagger}$	46	7.591	7.547	7.49	1.354	0.770
136	$Xe^{\dagger}$	60	20.767	20.786	23.01	−9.747	−9.663
58	$Ni^{\dagger}$	64	5.988	6.013	6.04	−0.846	−0.437
136	$Xe^{\dagger}$	87	16.722	16.797	17.69	−5.470	−5.044
58	$Ni^{\dagger}$	88	4.829	4.817	4.97	−2.816	−3.068
197	Au	117	31.338	28.169	29.56	6.016	−4.704
208	Pb	120.4	32.815	29.642	31.02	5.788	−4.439
209	Bi	157	28.047	26.532	27.41	2.325	−3.203
209	Bi^{*}	157	28.033	26.532	27.406	2.290	−3.188
209	Bi	162.8	27.177	26.058	27.03	0.546	−3.595
209	Bi	171	26.419	25.430	26.04	1.457	−2.341
209	Bi	183	25.576	24.595	25.01	2.265	−1.656
208	Pb	202.6	22.860	22.879	23.45	−2.512	−2.433
197	Au	255.7	18.918	19.058	19.49	−2.932	−2.212
136	$Xe^{\dagger}$	262	8.777	8.913	9.16	−4.172	−2.689
58	$Ni^{\dagger}$	264	2.366	2.375	2.41	−1.798	−1.443
209	Bi	269.6	20.368	20.456	21.18	−3.829	−3.417
197	Au	286.7	18.017	18.073	18.36	−1.863	−1.559
136	$Xe^{\dagger}$	433	6.914	7.030	7.1	−2.608	−0.983
209	Bi	498.6	15.471	15.953	16.42	−5.774	−2.841
18	O^{*}	690	0.125	0.124	0.123	1.776	0.943
136	Xe^{*}	780	5.651	5.757	5.806	−2.654	−0.829
209	Bi	866.7	13.160	13.691	13.78	−4.496	−0.639
238	U^{*}	900	16.062	16.823	16.739	−4.038	0.506
197	Au^{*}	950	11.655	12.134	12.086	−3.561	0.405
40	Ar^{*}	985	0.580	0.580	0.584	−0.558	−0.524

Table A.3: *Stopping powers for aluminum target*

A	proj	$E(MeV/u)$	G4	ATIMA	Exp	%G4	%ATIMA
58	$Ni^{\dagger}$	45	6.986	6.499	6.14	13.790	5.854
136	$Xe^{\dagger}$	60	18.791	17.738	19.12	−1.719	−7.223
58	$Ni^{\dagger}$	66	5.072	5.024	4.94	2.674	1.709
58	$Ni^{\dagger}$	88	4.153	4.129	4.23	−1.801	−2.377
136	$Xe^{\dagger}$	88	14.331	14.315	14.47	−0.957	−1.067
197	Au	110.9	26.385	24.924	25.56	3.230	−2.486
209	Bi	163.3	22.168	22.523	22.82	−2.854	−1.297
208	Pb	193.3	19.945	20.310	20.64	−3.365	−1.596
209	Bi	258.8	17.694	18.148	18.38	−3.731	−1.257
136	$Xe^{\dagger}$	259	7.659	7.797	8	−4.255	−2.532
197	Au	263.4	17.314	16.367	16.62	4.180	−1.522
58	$Ni^{\dagger}$	268	2.040	2.044	2.05	−0.479	−0.254
136	$Xe^{\dagger}$	433	6.033	6.136	6.22	−2.998	−1.339
209	Bi	495.2	13.479	14.000	14.36	−6.128	−2.501
136	Xe^{*}	780	4.985	5.003	5.077	−1.802	−1.451
209	Bi	874.7	11.543	11.978	12.17	−5.147	−1.569
238	U^{*}	900	14.129	14.75	14.703	−3.900	0.377
197	Au^{*}	950	10.312	10.630	10.572	−2.454	0.550
40	Ar^{*}	985	0.503	0.505	0.494	1.892	2.293

Table A.4: *Stopping powers for copper target*

A	proj	$E(MeV/u)$	G4	ATIMA	Exp	%G4	%ATIMA
58	$Ni^{\dagger}$	46	6.126	5.710	5.28	16.031	8.156
136	$Xe^{\dagger}$	60	16.850	15.902	17.12	−1.576	−7.113
58	$Ni^{\dagger}$	64	4.625	4.589	4.63	−0.100	−0.879
58	$Ni^{\dagger}$	87	3.751	3.733	3.78	−0.763	−1.219
136	$Xe^{\dagger}$	87	12.96	12.953	12.67	2.288	2.236
209	Bi	166.5	19.947	20.185	20.39	−2.169	−1.003
58	$Ni^{\dagger}$	251	1.905	1.918	1.92	−0.744	−0.058
209	Bi	261.6	15.995	16.394	16.58	−3.526	−1.119
136	$Xe^{\dagger}$	434	5.475	5.578	5.6	−2.227	−0.387
209	Bi	500.1	12.218	12.733	12.81	−4.620	−0.599
209	Bi	873.4	10.539	11.016	11.11	−5.139	−0.841

Table A.5: *Stopping powers for silver target*

A	proj	$E(MeV/u)$	G4	ATIMA	Exp	%G4	%ATIMA
58	$Ni^{\dagger}$	46	5.486	4.666	4.42	24.122	5.572
58	$Ni^{\dagger}$	62	4.215	3.867	3.87	8.936	−0.061
136	$Xe^{\dagger}$	62	14.746	12.930	14.16	4.142	−8.679
58	$Ni^{\dagger}$	87	3.189	3.110	3.18	0.306	−2.183
136	$Xe^{\dagger}$	87	11.406	10.817	10.56	8.018	2.438
209	Bi	165.8	17.149	17.161	17.25	−0.584	−0.512
209	Bi	260.4	13.712	14.055	14.12	−2.886	−0.458
136	$Xe^{\dagger}$	262	5.892	6.001	6.12	−3.713	−1.940
58	$Ni^{\dagger}$	268	1.574	1.577	1.59	−1.000	−0.779
136	$Xe^{\dagger}$	428	4.723	4.827	4.85	−2.612	−0.454
209	Bi	492.3	10.583	11.065	11.03	−4.044	0.324
209	Bi	851.6	9.188	9.623	9.66	−4.879	−0.378
238	U^{*}	900	11.217	11.821	11.728	−4.351	0.796

Table A.6: *Stopping powers for gold target*

A	proj	$E(MeV/u)$	G4	ATIMA	Exp	%G4	%ATIMA
197	Au	117.6	18.330	18.025	18.11	1.216	−0.466
209	Bi	186.4	15.872	15.964	16.12	−1.536	−0.963
197	Au	255.5	12.320	12.643	12.75	−3.367	−0.835
136	Xe^{*}	780	3.832	3.939	3.959	−3.192	−0.501
238	U^{*}	900	11.013	11.662	11.533	−4.506	1.119
197	Au^{*}	950	8	8.397	8.332	−3.984	0.781
40	Ar^{*}	985	0.396	0.395	0.389	1.921	1.751

Table A.7: *Stopping powers for lead target*

Bibliography

[1] http://www.gsi.de/forschung/kp/kp2/collaborations/R3B/index_e.html

[2] http://www.gsi.de/fair/

[3] http://www.gsi.de

[4] http://fpsalmon.usc.es/r3b/simulationIndex.shtml

[5] http://www.gsi.de/forschung/kp/kp2/collaborations/land/collaboration_e.html

[6] http://www-linux.gsi.de/ weick/atima/

[7] C. Rodríguez-Tajes: Diploma thesis *Characterization of the ALADIN setup at GSI for Coulomb Dissociation experiments.* Universidade de Santiago de Compostela. September 2006.

[8] Helmut Weick PhD thesis. *Einfluss der Umladung beim Abbremsen von Schwerionen im Energiebereich (100-1000)MeV/u.* Justus-Liebig-Universität Gießen. Darmstadt. October 2000

[9] Michael Maier PhD thesis. *New applications for slowing down of high-energy heavy ions* Justus-Liebig-Universität Gießen. Darmstadt. July 2004

[10] S. Typel, G. Baur. *Phys. Rev. C* **49**, 379 (1994)

[11] S. Typel, G. Baur. *Phys. Rev. C* **50**, 2104 (1994)

[12] F. Schümann et al. *Phys. Rev. Lett.* **90**, 232501 (2003)

[13] F. Schümann et al. *Phys. Rev. C* **73**, 015806 (2006)

[14] Y. Togano et al. *Eur. Phys. J. A* **27** s01, 233-236 (2006)